EBioMedicine 2 (2015) 1944–1956

Contents lists available at ScienceDirect

EBioMedicine

journal homepage: www.ebiomedicine.com

Research Article

PP2AC Level Determines Differential Programming of p38-TSC-mTOR Signaling and Therapeutic Response to p38-Targeted Therapy in Colorectal Cancer

Yanjie Zhang [a,b,*], Xiaowen Wang [a], Xiaoyu Qin [b], Xinxin Wang [b], Feng Liu [b], Eileen White [a,c], X.F. Steven Zheng [a,d,**]

[a] Rutgers Cancer Institute of New Jersey, Rutgers, the State University of New Jersey, 195 Little Albany Street, New Brunswick, NJ 08903, USA
[b] Oncology Department, Shanghai Ninth People's Hospital, Shanghai Jiaotong University School of Medicine, Shanghai 201900, China
[c] Department of Molecular Biology and Biochemistry, Rutgers University, 604 Allison Road, Piscataway, NJ 08854, USA
[d] Department of Pharmacology, Robert Wood Johnson Medical School, Rutgers University, 675 Hoes Lane, Piscataway, NJ 08854, USA

ARTICLE INFO

Article history:
Received 27 October 2015
Received in revised form 16 November 2015
Accepted 17 November 2015
Available online 19 November 2015

Keywords:
Targeted therapy
Cancer
Signal transduction
mTOR
p38
PDX

ABSTRACT

The p38 MAP kinase is a promising cancer drug target but its therapeutic effect is not fully understood. Here we report that the response of colorectal cancer (CRC) to p38 inhibitors (p38i) is highly variable: while p38i induces regression of one subgroup of CRCs, it stimulates growth of another subgroup. We further show that PP2AC is differentially expressed in the two different CRC subgroups, which determines the programing of p38-TSC-mTORC1 signaling through differential TSC2 phosphorylation at S664, 1254 and 1798, and the antitumor activity by p38i. Remarkably, modulation of PP2AC level is sufficient to reprogram p38-to-mTORC1 signaling and antitumor response. PP2AC expression accurately predicts therapeutic response to p38i in several CRC models, including a large cohort of patient-derived xenografts (PDXs). Moreover, we demonstrate that combination of p38 and mTOR kinase inhibitors effectively overcomes resistance to either inhibitor in single agent therapy. These results demonstrate that alternative routing of signal transduction underlies differential response to p38 and mTOR targeted therapies. The biomarker-guided therapeutic strategies described herein provide a compelling reason for testing in metastatic CRC patients who suffer very poor prognosis due to lack of efficacious drug therapies.

1. Introduction

Colorectal cancer (CRC) is a major global health concern, which accounts for 1,400,000 new cancer cases and nearly 700,000 deaths in 2012. It is prevalent in developed countries but has seen rapid rise in developing countries. Early stage CRC can be treated with combination of surgery and chemotherapy, which has good progression-free and overall survival rates. However, for metastatic CRC, the five-year survival rate is only 11% according to American Cancer Society. Standard systemic treatment is chemotherapy with cytotoxic drugs fluorouracil or capecitabine (Segal and Saltz, 2009). In recent years, targeted agents VEGF and EGFR inhibitors have been introduced (Misale et al., 2012). However, the overall death rate in metastatic CRC remains high because EGFR therapeutic antibodies Cetuximab and Panitumumab only benefit approximately 25% metastatic CRC patients (Misale et al., 2014). The remainder is refractory to EGFR targeted therapy mainly due to mutations in *K-RAS*, and in some cases *B-RAF* or *PIK3CA* (Misale et al., 2014). Because these patients suffer very poor prognosis, new systemic therapy is urgently needed to improve survival.

The p38 mitogen-activated protein kinases (MAPK) are key regulators of cellular responses to stress stimuli such as heat and osmotic shock, UV irradiation and inflammatory cytokines (Ashwell, 2006; Nebreda and Porras, 2000). There are four members in this MAPK subfamily: p38α, p38β, p38γ and p38δ. While p38α is ubiquitous, expression of other p38 isoforms is more restricted. p38 MAPK phosphorylates a myriad of substrates including transcription factors and kinases that mediate responses in inflammation, differentiation, cell cycle, apoptosis and cytokine production. Although much attention has been focused on p38 in inflammation, increasing evidence indicates that p38 is important for a number of other diseases including cancer (Han and Sun, 2007; Wagner and Nebreda, 2009). Elevated p38α activity occurs in CRC, mammary carcinomas, follicular lymphoma, glioma, head and neck squamous cell carcinomas, lung cancer, and thyroid cancer (Koul et al., 2013). In CRC, p38α and p38β (referred to as p38 hereafter) are especially essential for cancer cell proliferation and survival (Comes et al., 2007; Gupta et al., 2014). Genetic ablation or chemical inhibition

* Correspondence to: Y. Zhang, Oncology Department, Shanghai Ninth People's Hospital, Shanghai Jiaotong University School of Medicine, Shanghai 201900, China.
** Correspondence to: X.F. Steven Zheng, Rutgers Cancer Institute of New Jersey, Rutgers, the State University of New Jersey, 195 Little Albany Street, New Brunswick, NJ 08903, USA
E-mail addresses: zhangyanjie@shsmu.edu.cn (Y. Zhang), zhengst@cinj.rutgers.edu (X.F.S. Zheng).

http://dx.doi.org/10.1016/j.ebiom.2015.11.031

of p38 causes cell cycle arrest and apoptotic cell death in a cell type-specific manner. In addition, targeting p38α and p38β sensitizes CRC cells to 5-fluorouracil and overcomes irinotecan resistance (de la Cruz-Morcillo et al., 2012; Paillas et al., 2011).

p38 is a major therapeutic target for inflammatory diseases. Many selective p38α and p38β inhibitors (p38i) have been developed (Kumar et al., 2003). Although earlier trials with rheumatoid arthritis have not demonstrated superiority for this class of drugs over the standard care steroid treatment, promising clinical results have been obtained for acute coronary syndrome, atherosclerosis and chronic obstructive pulmonary disease (COPD). For example, a recent phase 2 clinical trial on acute coronary syndromes with an oral p38 inhibitor showed that the drug has achieved favorable clinical endpoints (Newby et al., 2014), which led to initiation of a large phase 3 trial involving 25,000 patients. As a result of a decade's effort by the pharmaceutical and biotech industry in this therapeutic space, a large collection of high quality p38is have been tested in humans and shown to have desirable pharmacological and toxicological profiles.

As p38 is essential for many human malignancies including CRC, some p38is have been tested in early stage human cancer clinical trials (https://clinicaltrials.gov). To date, however, positive results have not been reported. It has become clear that due to inter-patient and intra-patient heterogeneous nature of human tumors, only a subgroup(s) of any given cancer type would likely respond favorably to a particular p38i-targeted therapy. Clinical success of targeted therapies, as illustrated by EGFR inhibitors erlotinib and gefitinib, hinges upon a comprehensive understanding of the anticancer mechanism and reliable predictive biomarkers to identify the responders (Zhang et al., 2009). Currently, basic mechanistic insight into the sensitivity and resistance to p38is in cancer is needed. To this end, we investigated how CRCs respond to p38is. Our results provide insight into the molecular mechanisms for p38i sensitivity and resistance. More importantly, we identify a predictive biomarker of response to p38i to guide personalized therapy in different metastatic CRC subgroups.

2. Results

2.1. Opposing Effect of p38i on the Growth and Survival of Different Subgroups of CRCs

To evaluate therapeutic benefits of p38i, we examined the anticancer activity of SB202190, a selective inhibitor for p38α and p38β (Lee et al., 1994), on a panel of CRC cell lines. SB202190 attenuated growth of a subgroup of CRC cell lines such as RKO, CACO2 and SW480 in a dose- and time-dependent manner (Fig. 1A). SB202190 strongly inhibited colony formation and anchorage-independent growth (Fig. 1B and C) and elevated apoptotic cell death (Fig. 1D) in this same subset of CRC lines. In contrast, SB202190 surprisingly enhanced malignant growth and survival of another subgroup of CRC cell lines, HCT116, SW1116 and SW620 (Fig. 1A-D). The same therapeutic response was validated with xenograft tumors derived from SW480 and RKO, and HCT116 and SW620 cells (Fig. 1E-H) (No statistically significant animal weight fluctuations were observed in SB202190-treated groups compared with VC group, data not shown). LY2228820 and BIRB796, two other selective p38 inhibitors that have been tested in human clinical trials (Regan et al., 2003; Tate et al., 2013), exhibited similar therapeutic profiles to SB202190 (Supplementary Fig. 1), suggesting that the differential anti-CRC response was a common property for this class of p38 inhibitors.

2.2. CRC Subgroups have Opposing mTORC1 Signaling Responses to p38i

p38 has been shown to inhibit serum-stimulated mTORC1 signaling in immortalized murine embryonic fibroblasts (MEFs) (Li et al., 2003). To test if mTORC1 is involved in the antitumor response to p38i, we examined the effect of p38i on mTORC1 signaling in the two subgroups of CRCs. In RKO, CACO2 and SW480 cells, SB202190 abrogates phosphorylation of S6K1(T389) and S6(S235/236), but not AKT(S473), indicating that p38i selectively blocks mTORC1 signaling (Fig. 2A). In sharp contrast, SB202190 leads to a robust increase in phosphorylation of S6K1 and S6 in HCT116, SW1116 and SW620 cells (Fig. 2A), indicating that blockade of p38 signaling results in mTORC1 activation. Decreased AKT phosphorylation is seen in HCT116, SW1116 and SW620 cells, which can be explained by activation of the mTORC1-to-AKT negative feedback loop (Shi et al., 2005; Sun et al., 2005). The effect of SB202190 on mTORC1 signaling occurred rapidly and sustainably (Fig. 2B), which was also seen in SB202190-treated xenograft tumors (Fig. 2C-E). In all cases, excellent on-target p38 inhibition was achieved as indicated by blockage of phosphorylation of MK2 and p27, two established p38 substrates, in both drug-sensitive and -resistant CRC cells or tumors. Finally, LY2228820 and BIRB796 produced the same results as SB202190 (Fig. 2F). Thus, the differential effect on mTORC1 signaling is common to distinct p38i. Thus, the opposing effects of p38i on the two subgroups of CRCs are not due to variable p38 targeting efficiency. Instead, they reflect distinct intrinsic properties of individual CRCs.

2.3. p38i Targets Distinct TSC2 Phosphorylation Sites in Different Subgroups of CRCs

The tumor suppressor Tuberous Sclerosis Complex (TSC), consisting of TSC1 and TSC2 subunits, negatively regulates mTORC1 signaling by integrating diverse upstream growth and stress signals through phosphorylation of TSC2 at distinct sites by upstream kinases (Huang and Manning, 2008; Tee et al., 2003). In MEFs, SB202190 inhibited mTORC1 through MK2-dependent phosphorylation of TSC2 at S1254 (Li et al., 2003), and deletion of *TSC1* or *TSC2* abrogated this mTORC1 inhibition (Fig. 3A). Knockdown of *TSC1* or *TSC2* in CRC cells abrogated the negative or positive effect of SB202190 on mTORC1 signaling (Fig. 3B) or CRC growth (Fig. 3C). These results indicate that TSC is crucial for the therapeutic response to p38i in CRC.

TSC2 is phosphorylated at S1254, T1462, S664 and S1798 by MK2, AKT, ERK and RSK, respectively (Inoki et al., 2002; Li et al., 2003; Ma et al., 2005; Potter et al., 2002). In this role, RSK also serves as a downstream effector of ERK. To gain an insight into the differential effects by p38i, we investigated changes in TSC2 phosphorylation following SB202190 treatment in different CRC cells. In RKO, SW480 and $CACO_2$ cells, SB202190 blocked MK2-dependent TSC2 phosphorylation at S1254 (left panel in boxed area, Fig. 3D), without affecting AKT-, ERK- and RSK-dependent phosphorylation at T1462, S664 and S1798 (Fig. 3D). In contrast, in HCT116, SW1116 and SW620 cells, SB20219 enhanced ERK- and RSK-dependent TSC2 phosphorylation at S664 and S1798 (boxed area in right panel, Fig. 3D), but did not affect AKT- and MK2-dependent phosphorylations (Fig. 3D).

Consistently, SB202190 results in activation of ERK and RSK kinases in SW620 and HCT116 cells (Fig. 3E). To verify if ERK is involved, we treated SW620 and HCT116 cells with the MEK inhibitors PD98059 or U0126 in the absence or presence of SB202190. PD98059 and U0126 blunted ERK and RSK activation, enhanced TSC2 phosphorylation at S664 and S1798, and stimulated mTORC1 signaling by SB202190 (Fig. 3E). Together, these observations indicate that MK2 and ERK/RSK mediate the negative and positive effects of SB202190 on mTORC1 signaling through selective targeting of distinct TSC2 phosphorylation sites in p38i-inhibited and -stimulated CRC cell lines.

2.4. Combining p38 and mTOR Kinase Inhibitors Overcomes Resistance to either Drug Alone

Since mTORC1 activation correlated with p38i-mediated growth stimulation, this raises the possibility that targeting mTOR may counteract this response thereby restoring anti-tumor activity. ATP-competitive mTOR kinase inhibitors block signaling by both mTORC1 and mTORC2,

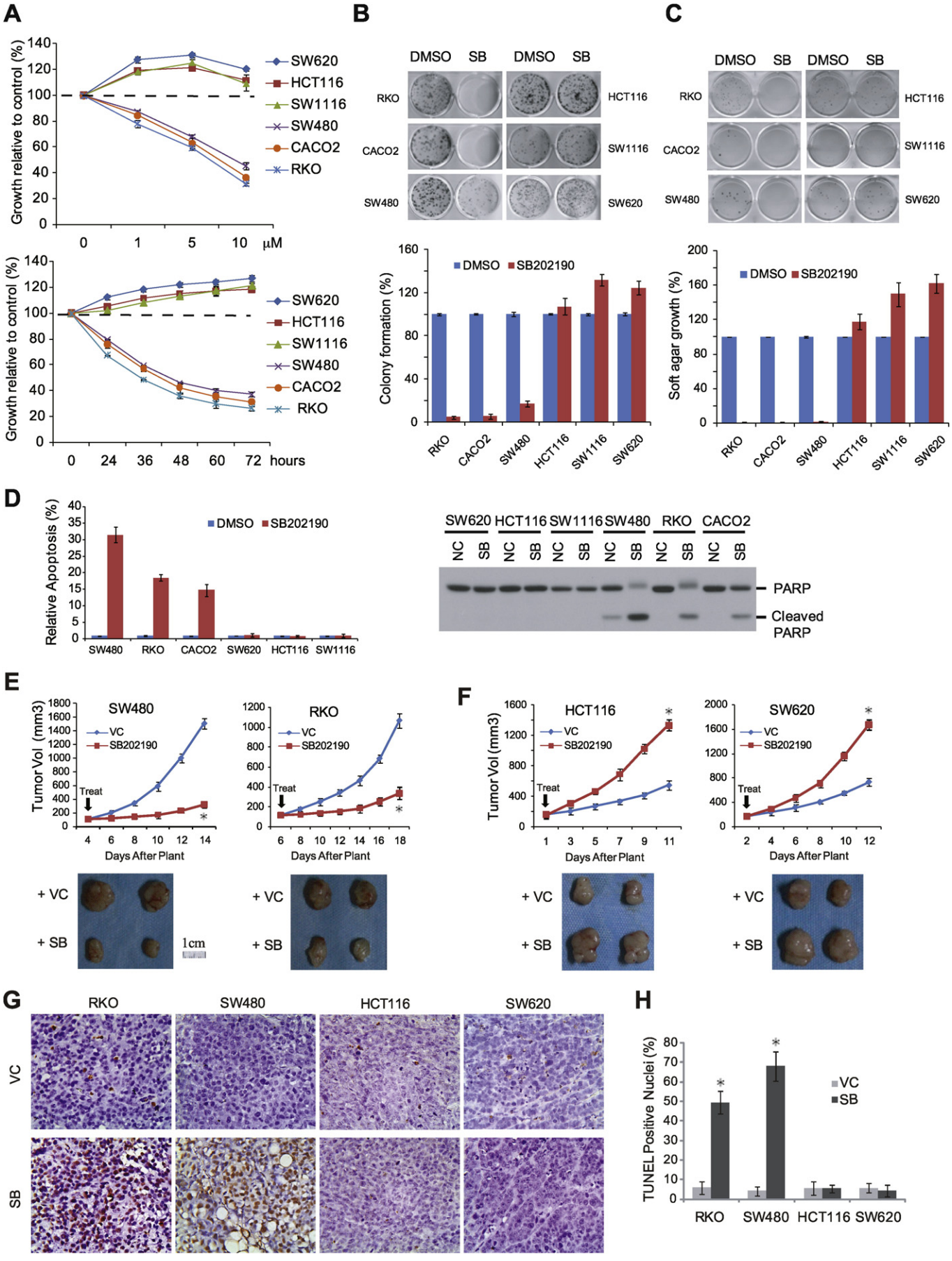
A
Growth relative to control (%)
SW620
HCT116
SW1116
SW480
CACO2
RKO
0 1 5 10 μM
Growth relative to control (%)
0 24 36 48 60 72 hours
B
DMSO SB DMSO SB
RKO HCT116
CACO2 SW1116
SW480 SW620
Colony formation (%)
DMSO SB202190
RKO CACO2 SW480 HCT116 SW1116 SW620
C
DMSO SB DMSO SB
RKO HCT116
CACO2 SW1116
SW480 SW620
Soft agar growth (%)
DMSO SB202190
RKO CACO2 SW480 HCT116 SW1116 SW620
D
Relative Apoptosis (%)
DMSO SB202190
SW480 RKO CACO2 SW620 HCT116 SW1116
SW620 HCT116 SW1116 SW480 RKO CACO2
NC SB NC SB NC SB NC SB NC SB NC SB
PARP
Cleaved PARP
E
SW480
RKO
Tumor Vol (mm3)
VC
SB202190
Treat
Days After Plant
+ VC
+ SB
1cm
F
HCT116
SW620
Tumor Vol (mm3)
VC
SB202190
Treat
Days After Plant
+ VC
+ SB
G
RKO SW480 HCT116 SW620
VC
SB
H
TUNEL Positive Nuclei (%)
VC
SB
RKO SW480 HCT116 SW620

which has the advantage over rapamycin analogs in preventing feedback activation of AKT (Zhang et al., 2011). We therefore examined BEZ-235 and OSI-027, two mTOR kinase inhibitors being tested in human clinical trials (Bhagwat et al., 2011). BEZ-235 and OSI-027 potently inhibited both mTORC1 and mTORC2, regardless whether p38i was present (Fig. 4A). mTOR kinase inhibitors abrogated SB202190-induced enhancement of CRC oncogenic growth as measured by SRB, colony formation and anchorage-independent growth assays (Supplementary Fig. 2, Fig. 4B and C), and they also elevated apoptotic cell death (Fig. 4D and E).

To assess the combination of p38 and mTOR kinase inhibitors in vivo, we generated SW620 xenograft tumors in nude mice and treated the tumor-bearing animals with a vehicle control (VC), SB202190 and OSI-027 individually or in combination. SB202190 achieved on-target inhibition as shown by diminished phosphorylation of MK2 and Hsp27 (Fig. 4F). As expected, OSI-027 blocked signaling by both mTORC1 and mTORC2 as shown by decreased phosphorylation of S6K1 and AKT (Fig. 4F). When SB202190 and OSI-027 were used in combination, all three kinases, p38, mTORC1 and mTORC2 were potently inhibited (Fig. 4F). While SB202190 alone enhanced SW620 xenograft tumor proliferation (Ki-67) and tumor burden (Fig. 4G and H), OSI-027 as a single agent did not have a discernible effect on SW620 tumor growth (Fig. 4G and H) (Zhang and Zheng, 2012). In sharp contrast, combining SB202190 and OSI-027 markedly attenuated xenograft tumor growth (Fig. 4G and H), and induced apoptosis of xenograft tumor cells (Fig. 4I). Taken together, these data demonstrate that combined use of mTOR and p38 kinase inhibitors restores anti-CRC tumor activity where there is an intrinsic lack of response to either drug alone.

2.5. Tumor-specific PP2AC Expression Determines Differential p38-to-mTORC1 Signaling

Protein phosphatase 2A (PP2A) is a serine/threonine protein phosphatase composed of three subunits, A, B and C (Janssens and Goris, 2001). It has been reported that p38 negatively regulates ERK in a PP2A-dependent manner in rat cardiac ventricular myocytes (Liu and Hofmann, 2004). However, how these two kinases crosstalk has not been examined in cancer. We investigated expression of three PP2A subunits in CRC cell lines. Interestingly, while the level of A and B subunits of PP2A was similar across different CRC cell lines, there was a marked difference in levels of the C subunit (PP2AC), which was expressed at a much lower level in p38i-inhibited than -stimulated CRC cells (Fig. 5A). PP2AC knockdown in HCT116 cells resulted in marked increase in activation of ERK and RSK, and their dependent TSC2 phosphorylation events at S664 and S1798, respectively, as well as mTORC1 activation (Fig. 5B). Activity of ERK and RSK was no longer responsive to SB202190 treatment after PP2AC knockdown (Fig. 5B). Remarkably, phosphorylation of S6K1 was now inhibited by SB202190 (Fig. 5B). Interestingly, TSC2 phosphorylation at S1254 by MK2 was significantly increased by PP2AC knockdown, which was inhibited by SB202190 (Fig. 5B). These observations indicate that down-regulation of PP2AC leads to re-programming of p38-to-mTOR signaling from p38-ERK-RSK-TSC2-mTORC1 to p38-MK2-TSC2-mTORC1. Essentially the same results were obtained with SW620 cells (Fig. 5C), suggesting that the PP2AC-dependent signaling reprogramming is common phenomenon.

To explore the relationship between PP2AC expression and p38 signaling, we ectopically expressed PP2AC in RKO and SW480 cells, CRC cells with low endogenous PP2AC. In contrast to PP2AC knockdown, PP2AC overexpression significantly decreased activity of ERK and RSK, with concomitant reduction in phosphorylation of TSC2 at S664 and S1798 (Fig. 5D). Remarkably, SB202190 treatment now caused activation of ERK and RSK, which was accompanied by a concomitant increase in TSC2 phosphorylation at S664 and S1798, and phosphorylation of S6K and S6 (Fig. 5D). Thus, increasing the level of PP2AC in CRC cells with low endogenous PP2AC leads to reprogramming of p38-to-mTORC1 signaling from p38-MK2-TSC2-mTORC1 to p38-ERK-RSK-TSC2-mTORC1. Taken together, these observations demonstrate that the level of PP2AC is a major determinant of differential p38-to-mTORC1 signaling that can be reprogrammed by modulation of PP2AC expression. In response to SB202190, the binding of ERK to PP2AC was markedly decreased in HCT116 and SW620 cells, but not in SW480 and RKO cells (Fig. 5E). Thus when PP2AC expression is high, the binding of ERK to PP2AC is dependent on p38, and inhibition of p38 results in dissociation of the ERK-PP2AC complex and hence activation of ERK kinase.

2.6. PP2AC Expression Predicts the Outcome of p38-targeted Therapy in Patient-derived Xenografts (PDXs)

To investigate the significance and application of these findings, we asked if PP2AC has a similarly heterogeneous expression in primary human CRC tumors by immunohistochemistry (IHC) staining of primary tumors from 75 cases of malignant infiltrating CRCs. Indeed, IHC scores varied considerably, ranging from 0 to 300 (Fig. 5F and G), suggesting that PP2AC is a potentially useful biomarker for p38i-targeted therapy. Patient-derived xenograft (PDX) tumors are known to closely resemble primary tumors. Their use has transformed anticancer drug research, enabling study of therapeutic responses in a patient-relevant setting and accelerating the process from bench to clinic (Aparicio et al., 2015; Morton and Houghton, 2007). We developed 40 early passage PDX CRC tumors. H&E staining showed that these PDXs displayed histological features characteristic of primary human CRCs such as complex glandular tumor structures and tumor stroma (Fig. 6A, Supplementary Fig. 3A and B) (Fleming et al., 2012), which were absent from xenografted cancer cell lines, indicating that the PDXs are closely related to the primary CRCs.

We next carried out IHC staining analysis of the PDX tumors for PP2AC expression, which show highly variable PP2AC levels in different tumors. 9 PDX tumors (cases 1, 12, 13, 14, 17, 25, 26, 33, 34) with low PP2AC level (H-Score < 100) and 9 PDX tumors (cases 2, 3, 8, 11, 19, 28, 30, 31, 40) with high PP2AC level (H-Score > 200) were selected for further analysis (Fig. 6A, Supplementary Fig. 3A and B). PP2AC expression was further verified by immunofluorescence (IF) staining (Fig. 6A and Supplementary Fig. 3C). These two groups of PDX-bearing mice were treated with SB202190 at 5 mg/kg daily. SB202190 strongly attenuated growth of low PP2AC-expressing PDX tumors and achieved tumor regression in many cases (Fig. 6B and C, Supplementary Fig. 4). In sharp contrast, SB202190 not only failed to inhibit growth of high PP2AC-expressing PDX tumors, but also enhanced growth of these tumors in majority of the cases (Fig. 6D and E, Supplementary Fig. 5).

The differences in antitumor response are further clearly indicated by the T/C values, which were at or below 0 for majority of the low PP2AC expression PDX tumor group (0, complete growth inhibition; <0, tumor regression) (Fig. 6F). In contrast, T/C value was at or above

Fig. 1. Opposite effects of p38 targeting on growth and survival of different CRC cells and tumors. **A.** Top panel: CRC cells were treated with various concentrations of SB202190 for 48 h. Lower panel: CRC cells were treated with SB202190 at 10 μM for different times. Cell growth was measured by SRB assay (means ± s.d. in triplet, n = 3 in triplet). **B.** CRC cells were treated with SB202190 10 μM for 7–10 days and measured for formed colonies. Lower panel shows quantification (means ± s.d., n = 3 in triplet). **C.** CRC cells were treated with SB202190 10 μM for 2–4 weeks and measured for anchorage-independent growth in soft agar. Lower panel shows quantification (means ± s.d., n = 3 in triplet). **D.** CRC cells were treated with SB202190 10 μM for 72 h and analyzed for viability by Acridine Orange Staining or PARP cleavage. Left panel, quantification of staining results (means ± s.d., n = 3 in triplet); Right panel, immunoblot analysis of PARP cleavage. **E.** Nude mice bearing SW480 and RKO xenograft tumors were treated with SB202190 (5 mg/kg/day) or drug vehicle (VC). Tumor volumes were measured (means ± s.d., n = 6). *P < 0.01 versus VC. **F.** Nude mice bearing HCT116 and SW620 xenograft tumors were treated with SB202190 or drug VC and measured for tumor volumes (means ± s.d., n = 6). *P < 0.01 versus VC. **G.** Apoptosis in xenograft tumors treated with SB202190 or VC were analyzed by TUNEL staining. Shown are representative microscopic fields (400×). **H.** Quantification of TUNEL staining results (means ± s.d., n = 6). *P < 0.01 versus VC.

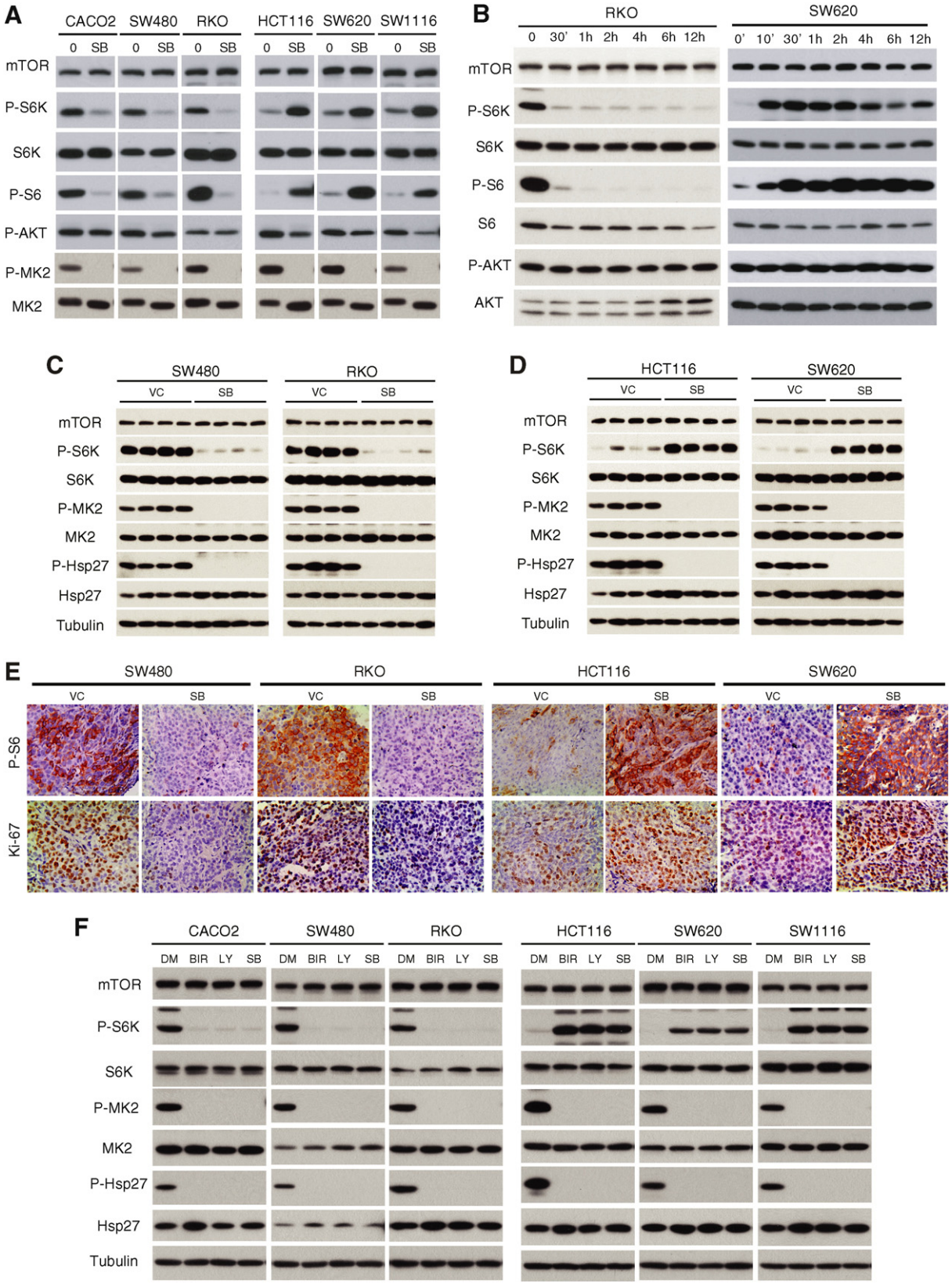

Fig. 2. Opposing effect of p38i on mTORC1 signaling in different CRCs. **A.** CRC cells were treated with 10 μM SB202190 for 2 h and analyzed for mTOR signaling and on-target inhibition of p38 by immunoblot. **B.** RKO and SW620 cells were treated with SB202190 10 μM for different times and analyzed for mTORC1 signaling by immunoblot. **C.** Nude mice bearing SW480 and RKO xenograft tumors were treated with SB202190 (5 mg/kg/day) or drug vehicle (VC), and analyzed for activity of mTORC1 and p38 signaling by immunoblot. Each lane represents an individual tumor sample. **D.** Nude mice bearing HCT116 and SW620 xenograft tumors were similarly analyzed as in Fig. 2C. **E.** CRC xenograft tumors were analyzed for P-S6 and Ki67 by IHC. Representative microscopic fields of P-S6 and Ki67 staining are shown (400×). **F.** CRC cells were treated with 4 μM LY2228820, 10 μM BIRB796 or 10 μM SB202190 for 2 h and p38 and mTORC1 signaling was analyzed by immunoblot.

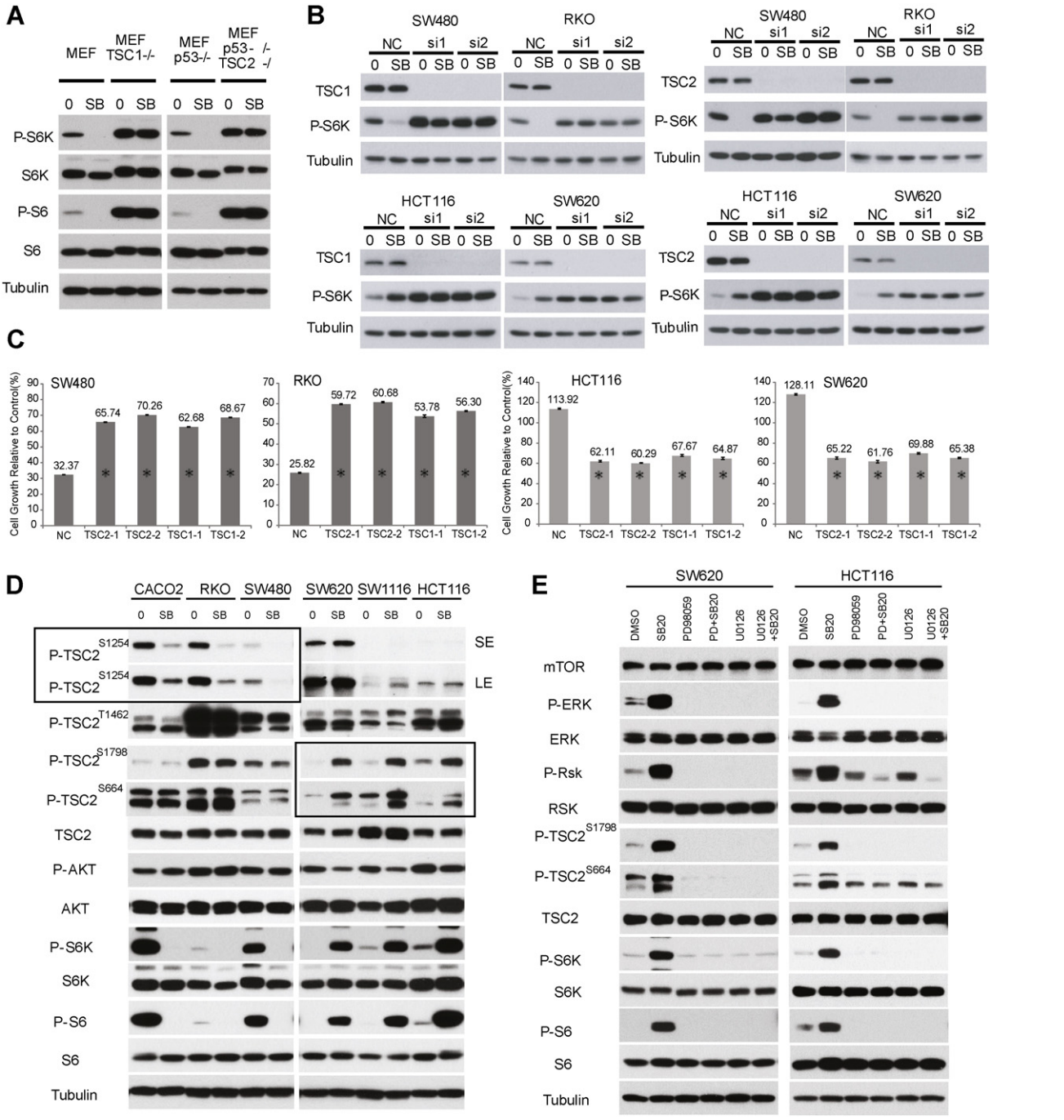

Fig. 3. p38 targets distinct phosphorylation sites of TSC2 in different CRC cell lines. **A.** *WT*, *TSC1*$^{-/-}$ or *TSC2*$^{-/-}$ MEF cells were treated with 10 μM SB202190 for 2 h and analyzed for P-S6K1 and P-S6 by immunoblot. **B.** CRC cells were transfected with two different *TSC1* or *TSC2* siRNAs, and then treated with 10 μM SB202190 for 2 h. TSC1, TSC2 and P-S6K1(T389) were analyzed by immunoblot. **C.** CRC cells were transfected with two different *TSC1* or *TSC2* siRNAs, and then treated with 10 μM SB202190 for 48 h. Cell growth was measured by SRB assay and expressed as percentage of SB202190/control (DMSO). Data represent means ± s.d. from three independent triplicate experiments. *P < 0.01 versus NC. **D.** Drug-sensitive CACO2, SW480 and RKO cells, and drug-resistant HCT116, SW620 and SW1116 cells were treated with 10 μM SB202190 for 2 h and analyzed for phosphorylation of TSC2 at S664, S1254, T1462 and S1798 by immunoblot. Boxed area highlights the different effects of SB202190 on TSC2 phosphorylation in drug-sensitive versus -resistant CRC cells. SE, short exposure, LE, long exposure. **E.** HCT116 and SW620 cells were treated with 10 μM SB202190 with or without Mek inhibitors 30 μM PD98059 or 10 μM U0126 for 2 h, and then analyzed for phosphorylation of TSC2, ERK, RSK, S6K1 and S6 by immunoblot.

100 for the high PP2AC expression group (100, no growth inhibition; >100, enhanced growth). SB202190 had excellent on-target inhibition of p38 in both groups of tumors, as shown by marked decrease in P-MK2 staining (Fig. 6G). However, it inhibited mTORC1 signaling (P-S6) and tumor cell proliferation (Ki67) in the low PP2AC expression group, but enhanced mTORC1 signaling and proliferation in the high PP2AC group (Fig. 6G). Essentially the same results are obtained with LY2228820, another p38 inhibitor (Supplementary Fig. 6). These results demonstrate that in the highly patient-relevant PDX CRCs, PP2AC expression reliably predicts the response of targeting p38 for both mTORC1 signaling and therapeutic outcome.

3. Discussion

In this study, we found that there is considerable variability in therapeutic response of CRCs to p38-targeted therapy. CRC tumors

with low PP2AC expression are highly sensitive to p38i, which represent an estimated 20% CRCs. In contrast, for CRCs with high PP2AC expression, p38i treatment promotes tumor growth. Thus caution must be taken because p38 targeting in this group of patients may worsen the therapeutic outcome. Differential programing of p38-to-mTORC1 signaling underlies the sensitivity and resistance of CRCs to p38-targeted therapy (Fig. 7). Although p38 can regulate mTORC1 activity through two distinct signaling axes, p38-MK2-TSC2-mTORC2 plays a dominant

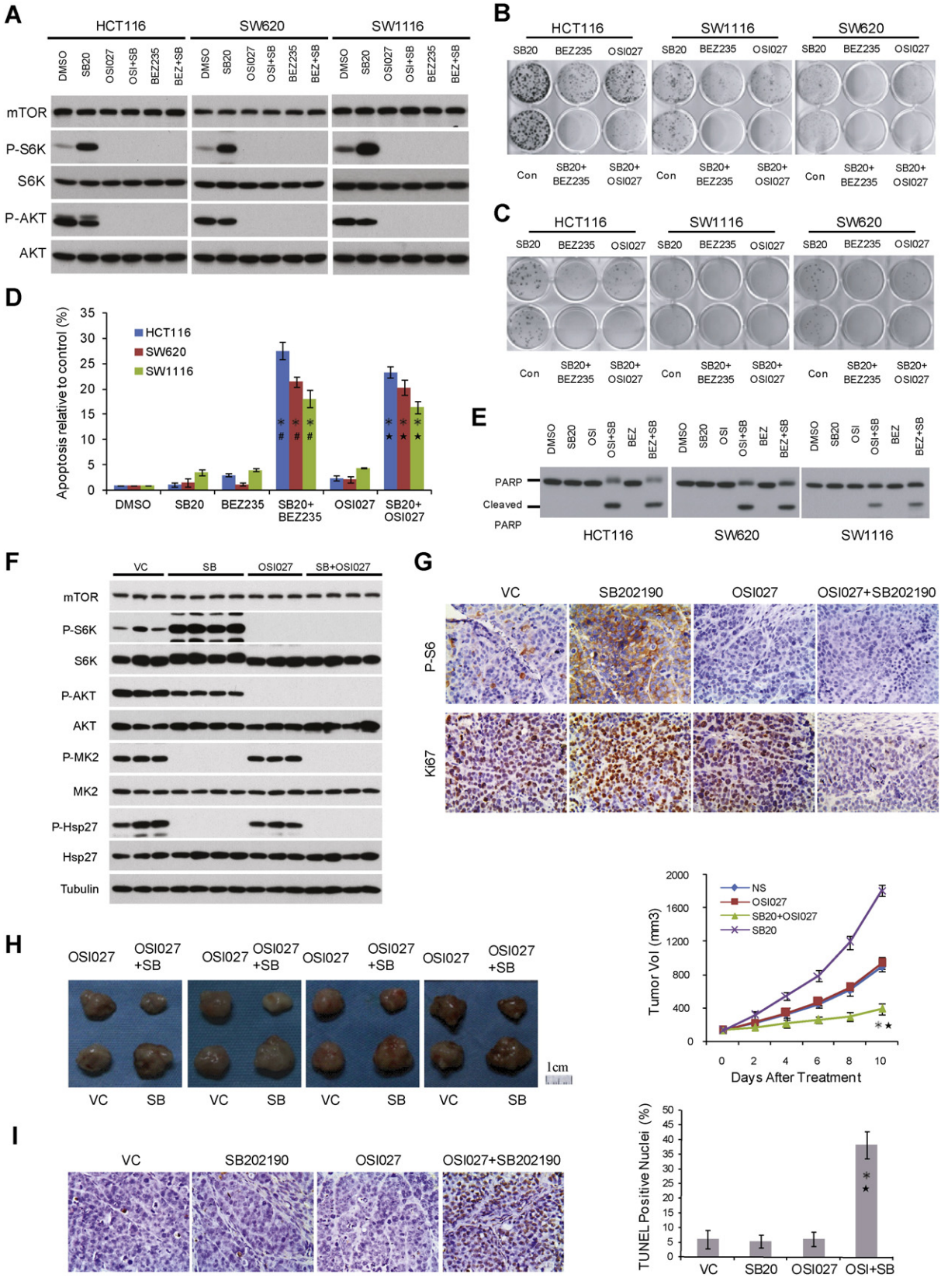

role in regulating mTORC1 activity in tumors with low PP2AC expression. In this group of CRCs, p38i leads to decreased phosphorylation of TSC2 at S1254 by MK2, inhibition of mTORC1 signaling, and inhibition of tumor cell survival and tumor growth. It is noteworthy that p38i induces extensive apoptotic cell death in the p38i-inhibited CRCs, which correlates with tumor regression. These observations provide compelling argument for initiation of biomarker-guided (PP2AC low), single agent p38i clinical trials for treating malignant CRCs where there is an urgent need of efficacious systemic drug therapy.

In CRCs with high PP2AC expression, the signaling flow from p38 to mTORC1 is mainly mediated by ERK- and RSK-dependent TSC2 phosphorylation at S664 and S1798, respectively. Treatment of these CRCs with p38i stimulates TSC2 phosphorylation at S664 and S1798, resulting in activation of mTORC1, and enhancement of CRC growth and survival. Remarkably, even though these tumors do not regress when treated with p38 and mTOR kinase inhibitors individually, they become highly sensitive to the combination of both inhibitors, which not only blunts tumor growth but also promotes apoptotic cell death. This observation suggests that p38i-induced mTORC1 activation renders CRC cells addicted to the mTORC1 pathway and thus susceptible to mTOR kinase inhibitors. Combinational therapy for this group of CRCs can greatly expand the utility of p38 and mTOR kinase inhibitors, neither of which has yet made meaningful impact in oncology.

These results illustrate the complexity of the tumor growth signaling network. Distinct routing of the same two signaling endpoints can have drastically different outcomes for targeted therapy. We demonstrate that p38 signal transduction to mTORC1 is determined by PP2AC levels with a strong inverse-correlation with therapeutic outcome of p38i in a large cohort of PDXs. Thus, PP2AC can be an excellent predictive biomarker for selecting patients for clinical trials with p38i in single agent therapy or in combination with an mTOR kinase inhibitor. CRC is the second leading cancer-related death in the United States. Nearly 50% CRC patients, when diagnosed, are already at the advanced metastatic stage and suffer dismal prognosis (Fakih, 2015). In recent years, anti-epidermal growth factor receptor (EGFR) antibodies cetuximab and panitumumab, in conjunction with traditional chemotherapeutic agent fluorouracil (5-FU), have extended the overall survival of some metastatic CRC patients from 12 to 24 months. Unfortunately, the majority of late stage CRCs carry *K-RAS*, *N-RAS*, *B-RAF* or *PIK3CA* mutations that confer resistance to the anti-EGFR therapy (Misale et al., 2014). Therefore, new systemic therapies are urgently needed. Interestingly, HCT16, RKO, SW480, SW620 and SW1116 cells all carry one or more mutations in *K-RAS*, *B-RAF* and *PIK3CA*. As shown here, these CRCs have excellent responses to either p38i alone or the combination of p38 and mTOR kinase inhibitors. It is compelling to test p38i in clinical settings using a biomarker-guided approach, which may bring efficacious therapeutic options for these needy patients.

4. Methods

4.1. Cell Lines, Cell Culture and Chemicals

Human colorectal cancer (CRC) cell lines (CACO-2, HCT116, RKO, SW1116, SW480 and SW620) were purchased from ATCC and cultured according to ATCC instructions. Wild type, TSC1$^{-/-}$, TSC2$^{+/+}$ p53$^{-/-}$, TSC2$^{-/-}$ p53$^{-/-}$ mouse embryonic fibroblast (MEF) cells (Zhang et al., 2003) were cultured in DMEM with 10% fetal bovine serum. SB202190, LY2228820, BIRB 796, OSI027 and BEZ235 were obtained from Selleckchem and MedChem Express; U0126 and PD98059 were purchased from Cell Signaling Technology. EDTA-free Complete Protease Inhibitor Cocktail and PhosSTOP were obtained from Roche. All cell lines have been tested to be free of mycoplasma contamination.

4.2. Experimental Animals

Housing and all procedures using BALB/c nude mice were approved by the Institutional Animal Care and Use Committee and in accordance with the Animals (Scientific Procedures) Act, 1986 (UK) (amended 2013). All sections of this report adhere to the ARRIVE Guidelines for reporting animal research. All mice were housed in individually ventilated cages (5 per cage) under specific pathogen free (SPF) condition. Housing was temperature-controlled, with a 12-h/12-h light/dark cycle. Animal weights were measured every other day.

4.3. Antibodies, Western Blot and Immunoprecipitation

Antibodies are purchased from the following vendors: P-TSC2(S1798) (sc-293149), Santa-Cruz Biotechnology; P-TSC2(S664) (ab133465) and S6K1 (ab32529), Abcam; PP2AA (#2041), PP2AB (#2290), PP2AC (#2059), P-S6K1(T398) (#9234), P-AKT(S473) (#4060), AKT (#9272), P-MK2(T334) (#3007), MK2 (#3042), P-Hsp27 (S82) (#9709), Hsp27 (#2402), P-S6(S235/236) (#4858), S6 (#2217), P-ERK(T202/Y204) (#4370), ERK (#4695), P-RSK(S380) (#9335), RSK (#9355), P-TSC2 (S1254) (#3616), P-TSC2(T1462) (#3617), TSC2 (#4308), mTOR (#2983), PARP (#9532), Ki67 (#9449), and Tubulin (#3873), Cell Signaling Technology; HRP-labeled anti-mouse and anti-rabbit secondary antibodies, Santa-Cruz Biotechnology and Alexa Fluor 594 conjugated secondary antibody, Invitrogen. Western blot analysis was performed as described previously (Thomas et al., 2014). For immunoprecipitation, CRC cells were treated with SB202190 10 μM for 2 h prior to lysis. Then cells were lysed with NP40 lysis buffer (50 mM Tris–HCl at pH 8.0, 150 mM NaCl, 5 mM EDTA, 0.5% NP40), and diluted lysates were applied to immunoprecipitation with anti-PP2AC antibody and immunoblotting with anti- ERK and anti-PP2AC antibody.

4.4. siRNA and Plasmids

siRNA for human PP2AC, TSC1 and TSC2 were designed and synthesized by OriGene Technologies (MD, USA). To confirm the target gene knock down effect, 2–4 oligonucleotides targeting different mRNA site were used for each gene. siRNA sequences are as follows:

TSC2-1: 5′-AUGUUCAGCAGAAUGUCCCTT.
TSC2-2: 5′-UAAACUCCGUCUGUUUACCTT.
TSC1-1: 5′-UAUUUAACAACAUCAGCCGTT.
TSC1-2: 5′-UUUAGGCUCUCAGAAAGGCTT.
PPP2AC-1: 5′-GGAUAGCAGCAAACAAUCAUUGGAG.
PPP2AC-2: 5′-UUUGUAUCUGGUGAUUUGCTT.
PPP2AC-3: 5′-AUAUCCCUCCAUCACUAGCTT.

Fig. 4. Combination of p38 and mTOR kinase inhibitors overcomes resistance to each drug as a single agent. **A.** CRC cells were treated with 10 μM SB202190 with or without 30 nM BEZ235 or 6 μM OSI027 for 2 h and analyzed for phosphorylation of S6K1 and AKT by immunoblot. **B.** CRC cells were treated with 10 μM SB202190 with or without 30 nM BEZ235 or 6 μM OSI027 and measured for colony formation. **C.** CRC cells were treated with 10 μM SB202190 with or without 30 nM BEZ235 or 6 μM OSI027 and measured for anchorage-independent growth. **D.** CRC cells were treated with 10 μM SB202190 with or without mTOR kinase inhibitor 30 nM BEZ235 or 6 μM OSI027 for 72 h and analyzed for cell death by Acridine Orange Staining. Data represent means ± s.d. from three independent triplicate experiments. *P < 0.01 versus SB202190 single treatment. #P < 0.01 versus BEZ235 single treatment.★P < 0.01 versus OSI027 single treatment. **E.** CRC cells were treated with 10 μM SB202190 with or without mTOR kinase inhibitor 30 nM BEZ235 or 6 μM OSI027 for 72 h and analyzed for PARP cleavage. **F.** SW620 xenograft tumors were treated with SB202190 and OSI027 individually or in combination. The effect on signaling by p38 (P-MK2 and P-Hsp27) and mTOR (P-S6K1 and P-AKT) was analyzed by immunoblot. **G.** Xenograft tumors were analyzed for P-S6 and Ki67 by IHC. Representative microscopic fields of P-S6 and Ki67 staining are shown (400×). **H.** Mice bearing SW620 xenograft tumors were treated with SB202190 and OSI027 individually or in combination. Tumor volume data are presented as means ± s.d. (n = 10). *P < 0.01 versus SB202190 single treatment. ★P < 0.01 versus OSI027 single treatment. **I.** Apoptosis of SW620 xenograft tumors treated with SB202190 and OSI027 individually or in combination (as above) was analyzed by TUNEL staining. Representative microscopic fields are shown (400×). Data are presented as means ± s.d. (n = 10). *P < 0.01 versus SB202190 single treatment. ★P < 0.01 versus OSI027 single treatment.

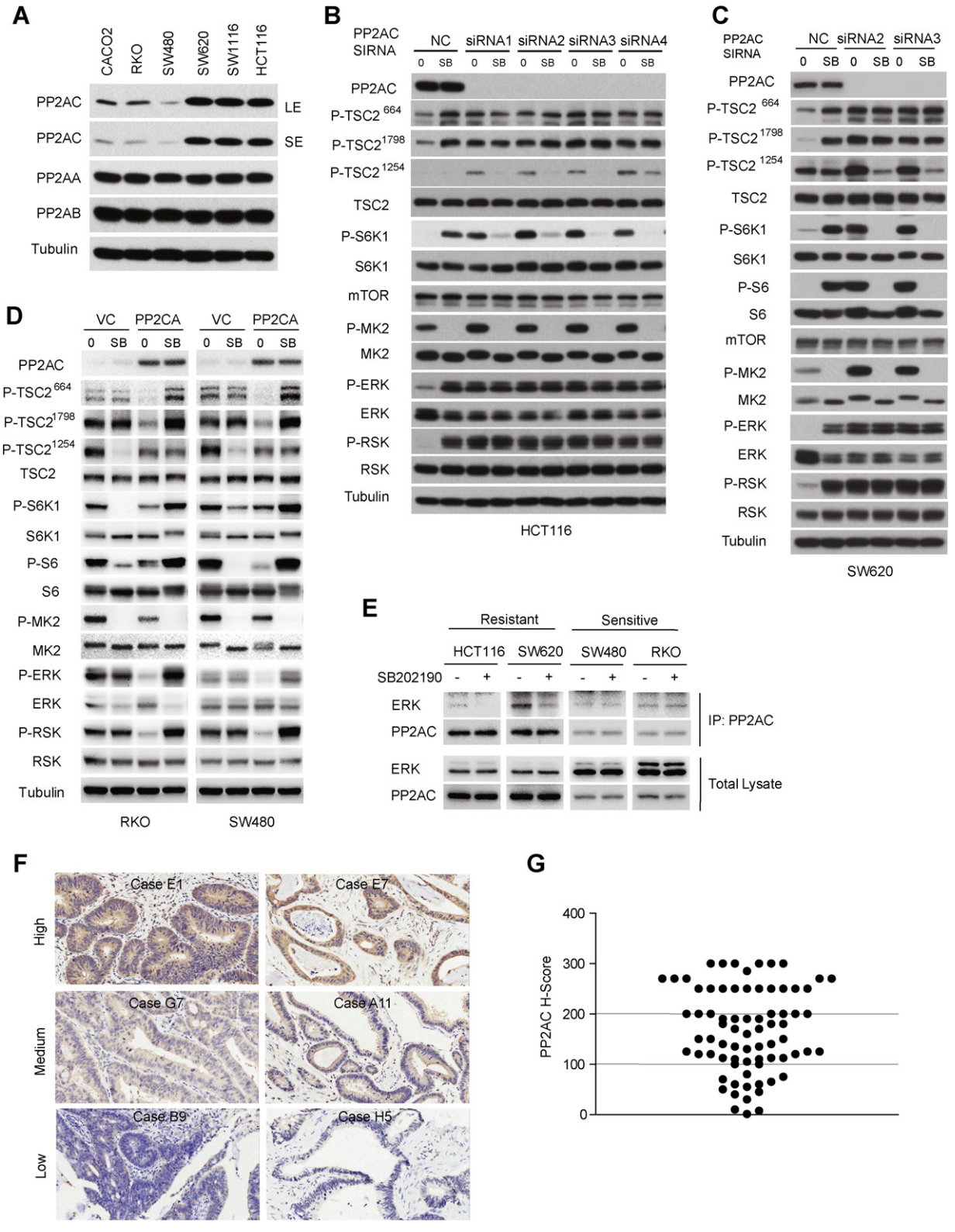

Fig. 5. PP2AC determines differential programming of p38-to-mTORC1 signaling. **A.** The protein level of PP2A-A, PP2A-B and PP2A-C in different CRC cells as analyzed by immunoblot. **B.** HCT116 cells were transfected with four different PP2AC siRNAs (1, 2, 3 and 4), and then treated with 10 μM SB202190 for 2 h. Phosphorylation of TSC2, S6K1, MK2, ERK and RSK was analyzed by immunoblot. **C.** SW620 cells were transfected with four different PP2AC siRNAs (1, 2, 3 and 4), and then treated with 10 μM SB202190 for 2 h. Phosphorylation of TSC2, S6K1, S6, MK2, ERK and RSK was analyzed by immunoblot. **D.** RKO and SW480 cells were transfected with PP2AC plasmid and then treated with 10 μM SB202190 for 2 h. Phosphorylation of TSC2, S6K1, S6, MK2, ERK and RSK was analyzed by immunoblot. **E.** Effect of p38i on ERK-PP2AC interaction in sensitive and resistant CRC cells. HCT116, SW620, SW480 and RKO cells were treated without or with 10 μM SB202190 for 2 h. Endogenous PP2AC was immunoprecipitated with a PP2AC-specific antibody and analyzed for binding to ERK by Western blot. **F.** Immunohistochemistry (IHC) staining of primary human CRC tissue microarray. Shown are staining of tumor tissue sections (400×) representative of high PP2AC, medium PP2AC and low PP2AC staining. **G.** PP2AC is differentially expressed in CRC. Scatter plot shows PP2AC staining level in individual tumor as H-score.

PPP2AC-4: 5′-ACCAUAUAUCGACCUAAUGGAAATG.
Control: 5′-UUCUCCGAACGUGUCACGUTT.

For siRNA transfection, CRC cells were incubated with siRNA oligonucleotides and Dharmacon transfection reagents for 16 h. Cell culture was then replenished with fresh culture medium. Cells were harvested 48 h post-transfection for immunoblot analysis. pcDNA-PP2AC plasmid was constructed by cloning PP2AC cDNA into pcDNA2 plasmid. Plasmid transfection was performed using Lipofectamine 2000 according to the manufacturer's protocol. Cells stably expressing PP2CA were selected in G418 for 2 weeks post plasmid transfection.

4.5. Cell Growth, Colony Formation, Anchorage-independent Growth and Apoptosis Assays

For SRB assay, cells were seeded in 96-well plates at an initial density of 3×10^3 cells/well. SRB assay was performed at 48 to 96 h post-seeding according to the manufacturer's protocols. For colony formation assay, 200 single cells were cultured in triplicates in a 12-well plate for 1–2 weeks, and stained by methylene blue. For soft agar colony formation assay, 500 cells were seeded in 0.35% Fisher low melt agar on a base of 0.7% Sigma agar in a 6-well plate. Culture dishes were transferred sequentially to a refrigerator (4 °C) for 15 min, to room temperature for 10 min, and then to the cell culture incubator. Agar cultures were stained with p-Iodonitroneotetrazolium violet (Sigma-Aldrich) for 2 hours, and then inspected and photographed using a MiniCount Colony Counter (Imaging Products International). For apoptosis assay, cells were stained with Acridine Orange (AO) and visualized using an inverted fluorescence microscope. Apoptotic cells were defined as cells showing cytoplasmic and nuclear shrinkage, and chromatin condensation or fragmentation. Apoptotic cell death was also detected by the PARP cleavage assay by immunoblot.

4.6. Immunohistochemistry (IHC), Immunofluorescence and TUNEL Assays

Streptavidin–Biotin Complex IHC method was used to detect Ki67, P-S6 (S235/236), P-MK2 (T334) and PP2AC. Primary antibodies were used at a concentration of 1:50 to 1:100. IHC signals were visualized with DAB (3,3-diaminobenzidine), using hematoxylin as a counter-staining. For immunofluorescence staining, Alexa Fluor 594 conjugated secondary antibody was used to detect the binding of primary antibodies. DAPI (4′,6-diamidino-2-phenylindole) was used to stain the nuclei. TUNEL assay was performed for detection of apoptotic cell death in situ according to the manufacturer's instructions (*In Situ* Cell Death Detection Kit, DAB; Roche Biotechnology). Apoptotic index was expressed as the percentage of TUNEL-positive nuclei/1000 cells.

4.7. Cell Line-derived Xenograft Tumors and Drug Therapy in Athymic Nude Mice

To generate xenograft tumors from CRC cell lines, a total of 5×10^6 to 1×10^7 cells in 100 ml PBS were injected subcutaneously into 4-week-old female BALB/c nude mice. After tumors were established, SB202190 was administered with 5 mg/kg SB202190 dissolved in DMSO and sterile saline by daily intraperitoneal injections for 10–12 days. For drug vehicle control, mice received daily injection of drug carrier. At least 6 mice were included in each treatment group. Tumor volume was measured using a Vernier caliper and calculated according to the formula: tumor volume (mm^3) = (length × width^2)/2. Tumor volume was measured every other day and is presented as means ± s.d. At the endpoint, mice were sacrificed, and tumors were removed and photographed and frozen in liquid nitrogen or fixed in formalin. Immunoblotting, IHC and TUNEL assay were performed to examine proliferation, cell signaling and apoptosis in xenograft tumor tissues.

For evaluating combination of SB202190 and OSI027, female BALB/c athymic nude mice (4–6 weeks old) were injected subcutaneously with 5×10^6 SW620 cells to establish the CRC xenograft model. After tumors were established, mice were randomized into four groups (10 animals per group) for 10 consecutive days of treatment: SB202190 was administered with 5 mg/kg SB202190 in DMSO and sterile saline by daily intraperitoneal injections, a safe dose as previously described (Lau et al., 2007); OSI-027 was administered at 10 mg/kg OSI-027 in DMSO and sterile saline by daily intraperitoneal injections, a dose well below previously established safe dose (Bhagwat et al., 2011); 5 mg/kg SB202190 plus 10 mg/kg OSI-027 were administered daily in DMSO and sterile saline by intraperitoneal injections; drug vehicle-treated mice received daily injection of identical solution without any drug (Wu et al., 2015; Zhang and Zheng, 2012). Tumor volume and tissue analysis were performed similarly.

4.8. IHC Staining of Malignant Infiltrating CRC Tumors

75 cases of de-identified malignant infiltrating CRC tumors were randomly obtained from Jan. 2013 to Jan. 2015. This study was carried out according to the provisions of the Helsinki Declaration of 1975. The Streptavidin–Biotin Complex (SABC) method was used in immunohistochemistry to detect PP2AC. Primary antibodies against PP2AC were used at a concentration of 1:300. To score a tumor cell as positive, cytoplasmic staining was counted. For the quantitative analysis, a Histo score (H-score) was calculated based on staining intensity and percentage of stained cells using the Aperio ScanScope® Systems (Vista, CA, USA). The intensity score was defined as follows: 0, no appreciable staining in cells; 1, weak staining in cells comparable to stromal cells; 2, intermediate staining; 3, strong staining. The fraction of positive cells was scored as 0–100%. The H-score was calculated by multiplying the intensity score and the fraction score, producing a total range of 0 to 300. For the purpose of data analysis, if H-score is more than 200, the tumor was classified as high PP2AC level. In contrast, if H-score is less than 100, the tumor was classified as low PP2AC level. Slides were examined and scored separately by two independent pathologists. Overall, PP2AC was highly expressed in 22 out of 75 CRC cases (29.33%), lowly expressed in 14 out of 75 cases (18.67%).

4.9. Patient Derived Xenograft (PDX) Tumors from Colorectal Cancer Tissues and Drug Sensitivity Assay

PDX tumors were generated as described previously (Li et al., 2007; Morton and Houghton, 2007). Briefly, samples of human colorectal adenocarcinomas were obtained within 30 min following surgical resection according to University Institutional Review Board (IRB)-approved protocols. Tumors were suspended in sterile RPMI 1640 and mechanically dissociated using scissors and then minced with a sterile scalpel blade over ice to yield $3 \times 3 \times 3$ mm^3 pieces. Non-necrotic tumor pieces were carefully selected and washed with serum-free PBS before implantation. Under anesthesia with Pelltobarbitalum Natricum, a 5-mm incision was made in the skin overlying the midabdomen of 5-week-old male BALB/c nude mice, and 2–3 tumor pieces were implanted together. The skin incision was closed with tissue adhesive (B. Braun Tissue Adhesive Histoacryl). Mice were monitored weekly for tumor growth for 16 weeks. When tumor size in the established primary tumor models (P0) reached 1500 mm^3, primary tumors were harvested and equally cut to small fragments of $3 \times 3 \times 3$ mm^3, and subcutaneously re-engrafted on the flank of 4–6 weeks old male Balb/c nude mice for expansion (P1). This process was repeated. Therapeutic assays with p38 inhibitor were performed on xenografts between P2 and P4. All procedures adhere to the BRISQ Guidelines for reporting preclinical research and were sterilely performed at the SPF facility. Human tissues used in laboratory studies do not meet the definition of human subject research per 45 CFR 46.102 since tissues were isolated from de-identified patient CRC tumors and have no identifiable private information.

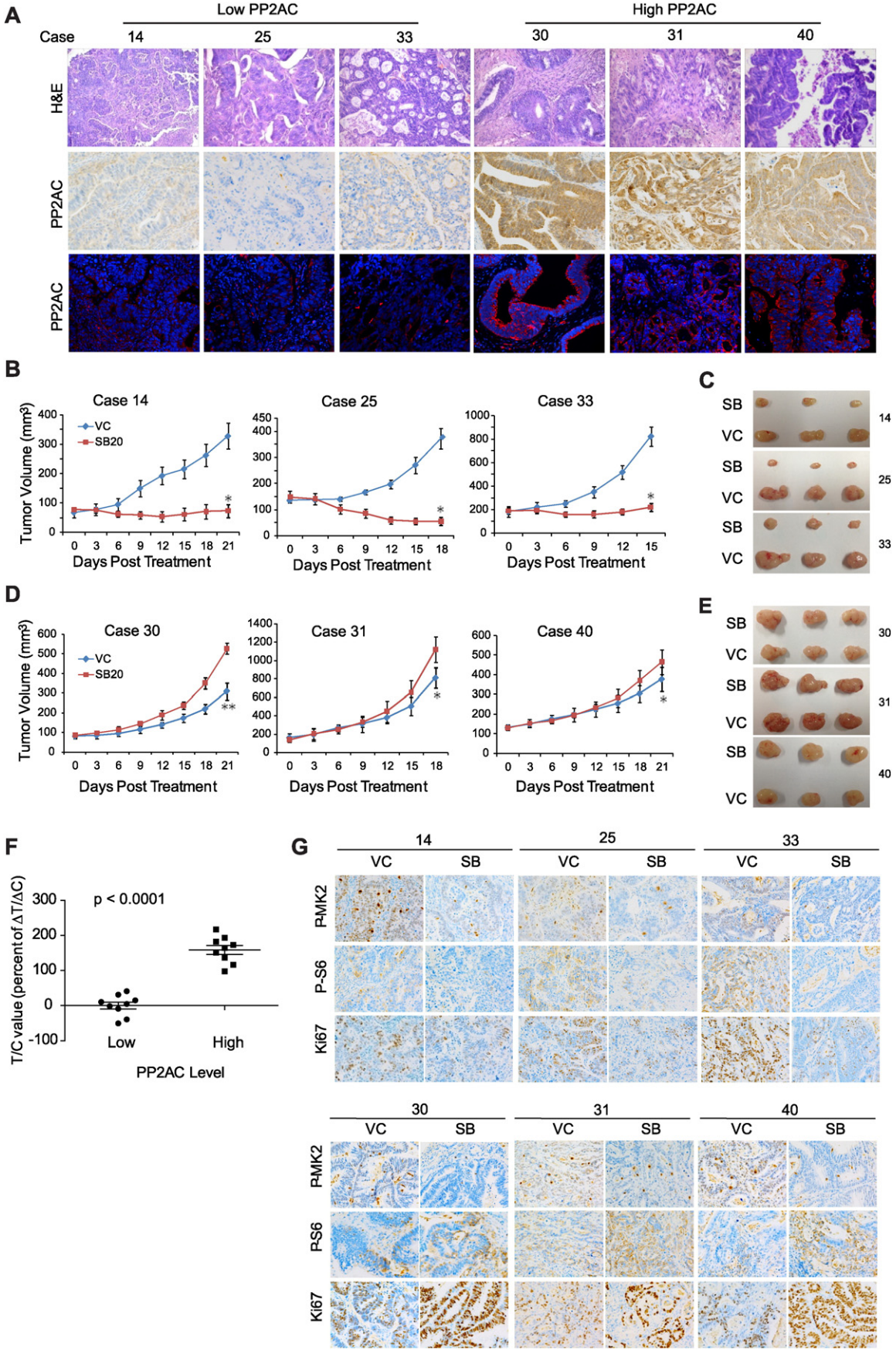
A
Low PP2AC
High PP2AC
Case
14
25
33
30
31
40
H&E
PP2AC
PP2AC
B
Case 14
Case 25
Case 33
VC
SB20
Tumor Volume (mm3)
Days Post Treatment
C
SB
VC
14
25
33
D
Case 30
Case 31
Case 40
E
F
p < 0.0001
T/C value (percent of ΔT/ΔC)
Low
High
PP2AC Level
G
VC
SB
PMK2
P-S6
Ki67
PS6

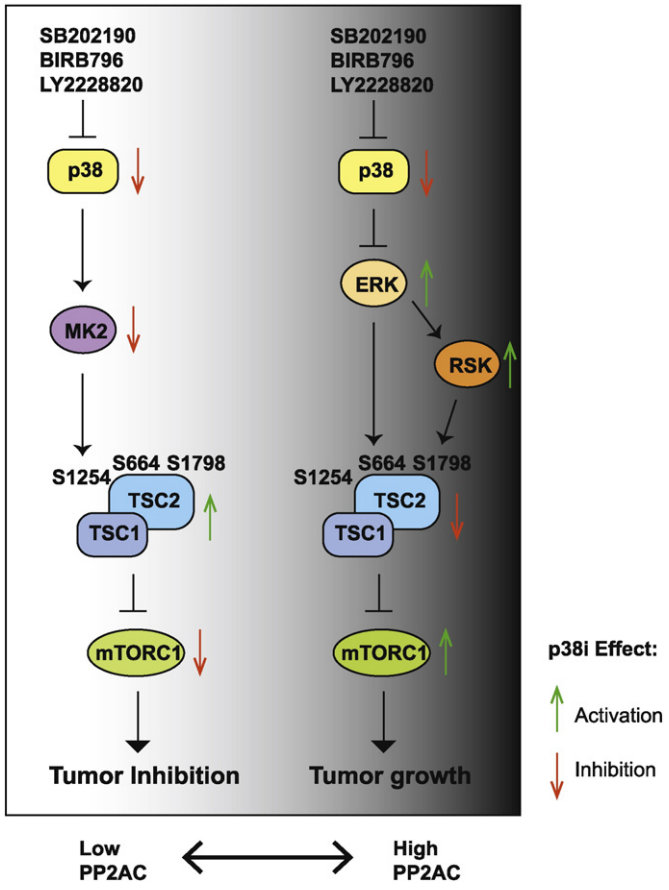

Fig. 7. A model showing differential programming of p38-to-mTORC1 signaling determines the outcome of p38-targeted therapies. It shows the primary signal transduction flow and effect of p38 inhibition on downstream effectors when PP2AC expression is low (left) or high (right) in CRCs.

Xenografts were allowed to grow until they reached a size of 100–200 mm^3 and then mice were randomized into two groups (6 animals per group) for treatment. SB202190 was administered with 5 mg/kg SB202190 or 10 mg/kg LY2228820 (Campbell et al., 2014) dissolved in DMSO and sterile saline by daily intraperitoneal injections for 15–24 consecutive days. Drug vehicle-treated mice received daily injection of identical solution without SB202190 or LY2228820. Tumor size was measured every 3 days by a digital caliper using the following formula: Tumor volume = (length × $width^2$)/2. T/C value (percent of ΔT/ΔC), the read out of tumor response to the treatment, was calculated as tumor volume change between the final and initial measurement date in Group SB20/ tumor volume change in Group VC. Investigators were blinded to the case number and correspondent PP2AC level during the experiment.

4.10. Statistical Analysis

Statistical analyses were carried out using the SAS 9.13 software. Data were expressed as means ± s.d. and were compared using one-way analysis of variance (ANOVA) followed by Student's *t* tests. Levene's Test was used to confirm the equality of variances between each data group. All statistical tests were conducted at a two-sided significance level of 0.05.

Conflict of Interests

The authors declare no known conflict of interests.

Acknowledgments

This work was supported by NIH R01 grants CA123391 and CA166575 (X.F.Z), and CA163591, CA188096 and CA130893 (E.W.), the National Nature Science Foundation of China 81270035 and Shanghai Pujiang Program 15PJ1404900 (Y.J.Z). Rutgers Cancer Institute of New Jersey Bioinformatics, Biospecimen, Histopathology and Animal Core Facilities were supported by NCI Cancer Center Support Grant P30-CA072720.

Appendix A. Supplementary Data

Supplementary data to this article can be found online at http://dx.doi.org/10.1016/j.ebiom.2015.11.031.

References

Aparicio, S., Hidalgo, M., Kung, A.L., 2015. Examining the utility of patient-derived xenograft mouse models. Nat. Rev. Cancer 15, 311–316.
Ashwell, J.D., 2006. The many paths to p38 mitogen-activated protein kinase activation in the immune system. Nat. Rev. Immunol. 6, 532–540.
Bhagwat, S.V., Gokhale, P.C., Crew, A.P., Cooke, A., Yao, Y., Mantis, C., Kahler, J., Workman, J., Bittner, M., Dudkin, L., et al., 2011. Preclinical characterization of OSI-027, a potent and selective inhibitor of mTORC1 and mTORC2: distinct from rapamycin. Mol. Cancer Ther.
Campbell, R.M., Anderson, B.D., Brooks, N.A., Brooks, H.B., Chan, E.M., De Dios, A., Gilmour, R., Graff, J.R., Jambrina, E., Mader, M., et al., 2014. Characterization of LY2228820 dimesylate, a potent and selective inhibitor of p38 MAPK with antitumor activity. Mol. Cancer Ther. 13, 364–374.
Comes, F., Matrone, A., Lastella, P., Nico, B., Susca, F.C., Bagnulo, R., Ingravallo, G., Modica, S., Lo Sasso, G., Moschetta, A., et al., 2007. A novel cell type-specific role of p38alpha in the control of autophagy and cell death in colorectal cancer cells. Cell Death Differ. 14, 693–702.
de la Cruz-Morcillo, M.A., Valero, M.L., Callejas-Valera, J.L., Arias-Gonzalez, L., Melgar-Rojas, P., Galan-Moya, E.M., Garcia-Gil, E., Garcia-Cano, J., Sanchez-Prieto, R., 2012. P38MAPK is a major determinant of the balance between apoptosis and autophagy triggered by 5-fluorouracil: implication in resistance. Oncogene 31, 1073–1085.
Fakih, M.G., 2015. Metastatic colorectal cancer: current state and future directions. J. Clin. Oncol. 33, 1809–1824.
Fleming, M., Ravula, S., Tatishchev, S.F., Wang, H.L., 2012. Colorectal carcinoma: pathologic aspects. J. Gastrointest. Oncol. 3, 153–173.
Gupta, J., del Barco Barrantes, I., Igea, A., Sakellariou, S., Pateras, I.S., Gorgoulis, V.G., Nebreda, A.R., 2014. Dual Function of p38α MAPK in Colon Cancer: Suppression of Colitis-Associated Tumor Initiation but Requirement for Cancer Cell Survival. Cancer Cell 25, 484–500.
Han, J., Sun, P., 2007. The Pathways to Tumor Suppression via Route p38. Trends Biochem. Sci. 32, 364–371.
Huang, J., Manning, B.D., 2008. The TSC1–TSC2 Complex: A Molecular Switchboard Controlling Cell Growth. Biochem. J. 412, 179–190.
Inoki, K., Li, Y., Zhu, T., Wu, J., Guan, K., 2002. TSC2 is Phosphorylated and Inhibited by Akt and Suppresses mTOR Signalling. Nat. Cell Biol. 4, 648–657.
Janssens, V., Goris, J., 2001. Protein Phosphatase 2A: A Highly Regulated Family of Serine/Threonine Phosphatases Implicated in Cell Growth and Signalling. Biochem. J. 353, 417–439.
Koul, H.K., Pal, M., Koul, S., 2013. Role of p38 MAP Kinase Signal Transduction in Solid Tumors. Genes Cancer 4, 342–359.
Kumar, S., Boehm, J., Lee, J.C., 2003. p38 MAP Kinases: Key Signalling Molecules as Therapeutic Targets for Inflammatory Diseases. Nat. Rev. Drug Discov. 2, 717–726.
Lau, J.M.C., Jin, X., Ren, J., Avery, J., DeBosch, B.J., Treskov, I., Lupu, T.S., Kovacs, A., Weinheimer, C., Muslin, A.J., 2007. The 14–3-3τ Phosphoserine-Binding Protein Is Required for Cardiomyocyte Survival. Mol. Cell. Biol. 27, 1455–1466.
Lee, J.C., Laydon, J.T., McDonnell, P.C., Gallagher, T.F., Kumar, S., Green, D., McNulty, D., Blumenthal, M.J., Keys, J.R., Land Vatter, S.W., et al., 1994. A Protein Kinase Involved in the Regulation of Inflammatory Cytokine Biosynthesis. Nature 372, 739–746.

Fig. 6. PP2AC predicts therapeutic outcome of p38i in patient-derived xenograft (PDX) CRC models. **A.** H&E staining, and IHC and IF staining of PP2AC in three representative PDX tumors (14, 25, 33) with low, and three representative PDX tumors (30, 31, 40) with high PP2AC expression. **B.** PDX tumors with low PP2AC expression are sensitive to SB202190. Mice bearing PDX tumors 14, 25 and 33 were treated with SB202190 or drug vehicle (VC) and measured for tumor volume (mean ± s.d., n = 6). *P < 0.01 versus VC. **C.** Representative p38i-sensitive PDX tumors at the end of the experiment. **D.** SB202190 enhances growth of PDX tumors with high PP2AC expression. Mice bearing PDX tumors 30, 31 and 40 were treated with SB202190 or drug vehicle (VC) and measured for tumor volume (mean ± s.d., n = 6). *P < 0.05, **P < 0.01 versus VC. **E.** Representative p38i-resistant PDX tumors at the end of the experiment. **F.** T/C value was calculated for the subgroup of 9 PDX tumors with low PP2AC expression and the subgroup of 9 PDX tumors with high PP2AC expression treated with SB202190 (t test, t = 9.903, df = 16, p < 0.0001). **G.** IHC staining of P-MK2, P-S6 and Ki67 in SB202190-treated PDX tumors 14, 25, 33 (upper panel), and 30, 31 and 40 (lower panel).

Li, Y., Inoki, K., Vacratsis, P., Guan, K.L., 2003. The p38 and MK2 Kinase Cascade Phosphorylates Tuberin, the Tuberous Sclerosis 2 Gene Product, and Enhances its Interaction with 14–3-3. J. Biol. Chem. 278, 13663–13671.
Li, C., Heidt, D.G., Dalerba, P., Burant, C.F., Zhang, L., Adsay, V., Wicha, M., Clarke, M.F., Simeone, D.M., 2007. Identification of Pancreatic Cancer Stem Cells. Cancer Res. 67, 1030–1037.
Liu, Q., Hofmann, P.A., 2004. Protein Phosphatase 2A-Mediated Cross-Talk Between p38 MAPK and ERK in Apoptosis of Cardiac Myocytes vol. 286.
Ma, L., Chen, Z., Erdjument-Bromage, H., Tempst, P., Pandolfi, P.P., 2005. Phosphorylation and Functional Inactivation of TSC2 by Erk Implications for Tuberous Sclerosis and Cancer Pathogenesis. Cell 121, 179–193.
Misale, S., Yaeger, R., Hobor, S., Scala, E., Janakiraman, M., Liska, D., Valtorta, E., Schiavo, R., Buscarino, M., Siravegna, G., et al., 2012. Emergence of KRAS Mutations and Acquired Resistance to Anti-EGFR Therapy in Colorectal Cancer. Nature 486, 532–536.
Misale, S., Di Nicolantonio, F., Sartore-Bianchi, A., Siena, S., Bardelli, A., 2014. Resistance to Anti-EGFR Therapy in Colorectal Cancer: From Heterogeneity to Convergent Evolution. Cancer Discov.
Morton, C.L., Houghton, P.J., 2007. Establishment of Human Tumor Xenografts in Immunodeficient Mice. Nat. Protoc. 2, 247–250.
Nebreda, A.R., Porras, A., 2000. p38 MAP Kinases: Beyond the Stress Response. Trends Biochem. Sci. 25, 257–260.
Newby, L.K., Marber, M.S., Melloni, C., Sarov-Blat, L., Aberle, L.H., Aylward, P.E., Cai, G., de Winter, R.J., Hamm, C.W., Heitner, J.F., et al., 2014. Losmapimod, a Novel p38 Mitogen-Activated Protein Kinase Inhibitor, in non-ST-Segment Elevation Myocardial Infarction: A Randomised Phase 2 Trial. Lancet 384, 1187–1195.
Paillas, S., Boissiere, F., Bibeau, F., Denouel, A., Mollevi, C., Causse, A., Denis, V., Vezzio-Vie, N., Marzi, L., Cortijo, C., et al., 2011. Targeting the p38 MAPK Pathway Inhibits Irinotecan Resistance in Colon Adenocarcinoma. Cancer Res. 71, 1041–1049.
Potter, C.J., Pedraza, L.G., Xu, T., 2002. Akt Regulates Growth by Directly Phosphorylating Tsc2. Nat. Cell Biol. 4, 658–665.
Regan, J., Pargellis, C.A., Cirillo, P.F., Gilmore, T., Hickey, E.R., Peet, G.W., Proto, A., Swinamer, A., Moss, N., 2003. The Kinetics of Binding to p38MAP Kinase by Analogues of BIRB 796. Bioorg. Med. Chem. Lett. 13, 3101–3104.
Segal, N.H., Saltz, L.B., 2009. Evolving Treatment of Advanced Colon Cancer. Annu. Rev. Med. 60, 207–219.
Shi, Y., Yan, H., Frost, P., Gera, J., Lichtenstein, A., 2005. Mammalian Target of Rapamycin Inhibitors Activate the AKT Kinase in Multiple Myeloma Cells by up-Regulating the Insulin-Like Growth Factor Receptor/Insulin Receptor Substrate-1/Phosphatidylinositol 3-Kinase Cascade. Mol. Cancer Ther. 4, 1533–1540.
Sun, S.-Y., Rosenberg, L.M., Wang, X., Zhou, Z., Yue, P., Fu, H., Khuri, F.R., 2005. Activation of Akt and eIF4E Survival Pathways by Rapamycin-Mediated Mammalian Target of Rapamycin Inhibition. Cancer Res. 65, 7052–7058.
Tate, C.M., Blosser, W., Wyss, L., Evans, G., Xue, Q., Pan, Y., Stancato, L., 2013. LY2228820 Dimesylate, a Selective Inhibitor of p38 Mitogen-Activated Protein Kinase, Reduces Angiogenic Endothelial Cord Formation in Vitro and in Vivo. J. Biol. Chem. 288, 6743–6753.
Tee, A., Manning, B., Roux, P., Cantley, L., Blenis, J., 2003. Tuberous Sclerosis Complex Gene Products, Tuberin and Hamartin, Control mTOR Signaling by Acting as a GTPase-Activating Protein Complex Toward Rheb. Curr. Biol. 13, 1259–1268.
Thomas, J.D., Zhang, Y.-J., Wei, Y.-H., Cho, J.-H., Morris, L.E., Wang, H.-Y., Zheng, X.F.S., 2014. Rab1A Is an mTORC1 Activator and a Colorectal Oncogene. Cancer Cell 26, 754–769.
Wagner, E.F., Nebreda, A.R., 2009. Signal Integration by JNK and p38 MAPK Pathways in Cancer Development. Nat. Rev. Cancer 9, 537–549.
Wu, T.-J., Wang, X., Zhang, Y., Meng, L., Kerrigan, J.E., Burley, S.K., Zheng, X.F.S., 2015. Identification of a Non-Gatekeeper Hot Spot for Drug-Resistant Mutations in mTOR Kinase. Cell Rep. 11, 446–459.
Zhang, Y., Zheng, X., 2012. mTOR-Independent 4E-BP1 Phosphorylation is Associated with Cancer Resistance to mTOR Kinase Inhibitors. Cell Cycle 11, 594–603.
Zhang, H., Cicchetti, G., Onda, H., Koon, H., Asrican, K., Bajraszewski, N., Vazquez, F., Carpenter, C., Kwiatkowski, D., 2003. Loss of Tsc1/Tsc2 Activates mTOR and Disrupts PI3K-Akt Signaling Through Downregulation of PDGFR. J. Clin. Invest. 112, 1223–1233.
Zhang, J., Yang, P.L., Gray, N.S., 2009. Targeting Cancer with Small Molecule Kinase Inhibitors. Nat. Rev. Cancer 9, 28–39.
Zhang, Y., Duan, Y., Zheng, X., 2011. Targeting the mTOR Kinase Domain: The Second Generation of mTOR Inhibitors. Drug Discov. Today 16, 325–331.